Polymer 49 (2008) 4017–4024

Contents lists available at ScienceDirect

Polymer

journal homepage: www.elsevier.com/locate/polymer

Synthesis and characterization of amorphous octakis-functionalized polyhedral oligomeric silsesquioxanes for polymer nanocomposites

Yuung-Ching Sheen [a], Chu-Hua Lu [a], Chih-Feng Huang [a], Shiao-Wei Kuo [b], Feng-Chih Chang [a,*]

[a] Institute of Applied Chemistry, National Chiao Tung University, 30010 Hsinchu, Taiwan, ROC
[b] Department of Materials Science and Engineering, National Sun Yat-Sen University, 804 Kaohsiung, Taiwan, ROC

ARTICLE INFO

Article history:
Received 10 May 2008
Received in revised form 24 June 2008
Accepted 27 June 2008
Available online 6 July 2008

Keywords:
Amorphous
Nanoparticles
Nanocomposites

ABSTRACT

We have synthesized the polyhedral oligomeric silsesquioxane (POSS) derivatives OS-POSS and OA-POSS through the hydrosilylation of styrene and 4-acetoxystyrene, respectively, with octakis(dimethylsiloxy)-silsesquioxane ($Q_8M_8^H$). We then prepared OP-POSS through acetoxyl hydrazinolysis of OA-POSS with hydrazine monohydrate. The chemical structures of these POSS derivatives were characterized using FTIR and ^{1}H NMR spectroscopy and MALDI-TOF mass spectrometry. Unlike $Q_8M_8^H$, which is crystalline, these three hydrosilylated POSS derivatives are liquids at 25 °C. Through DSC and XRD analyses, we found that they exhibit polymer-like glass transitions and amorphous halos. These octakis-functionalized POSS derivatives can be regarded as amorphous glasses possessing low glass transition temperatures, the values of which depend on the intermolecular interactions of their outer organic groups. To investigate the dispersion of these POSS derivatives in polymer nanocomposites, we blended OS-POSS, OA-POSS, and OP-POSS with polystyrene, poly(4-acetoxystyrene), and poly(4-vinylpyridine), respectively, and investigated the effects of the resulting intermolecular aromatic hydrophobic, dipole–dipole, and hydrogen-bonding interactions, respectively. Dipole–dipole interactions provided the best dispersion of OA-POSS in poly(4-acetoxystyrene), in which the POSS–polymer intermolecular interactions were of similar strength to the POSS–POSS interactions.

1. Introduction

When developing polymer nanocomposites, the attachment of organic groups to nanosized materials can have wide-ranging implications on the interactions occurring at the interfaces between the inorganic composite particles and the organic polymer matrices [1–5]. Polyhedral oligomeric silsesquioxane (POSS) derivatives possess well-defined chemical structures; they have the general formula of $(RSiO_{1.5})_8$, where the R units are organic groups located at the corners of an octahedral siloxane cube $(SiO_{1.5})_8$ (Fig. 1a) [7–12]. In addition to their high compatibility with polymers, POSS derivatives impart excellent thermal and mechanical properties to polymer nanocomposites. The presence of thermally stable POSS siloxane cores can prevent surface thermal degradation of polymeric matrices; microscopic POSS aggregation can result in hard domains that restrict polymer deformation during the application of an external force [6,8,9,13].

Although the molar masses of POSS derivatives can reach several thousands of Daltons (g/mol), depending on the size of the attached organic groups, most POSS derivatives can be theoretically

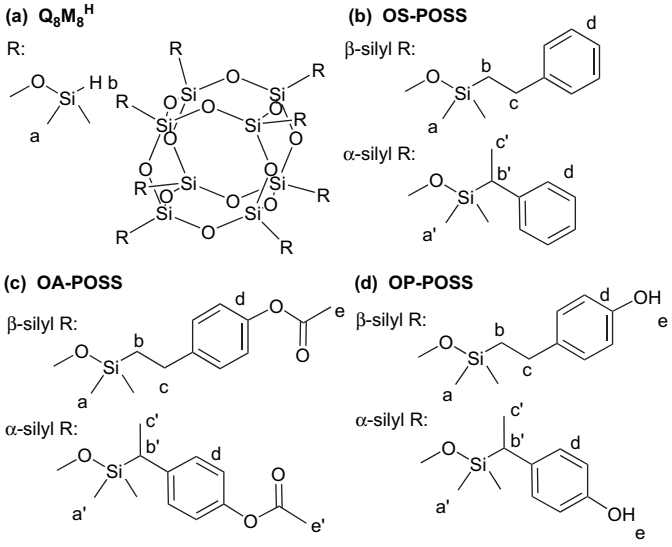

Fig. 1. Chemical structures of (a) $Q_8M_8^H$, (b) OS-POSS, (c) OA-POSS, and (d) OP-POSS and their assigned protons for analyzing the ^{1}H NMR spectra in Fig. 4.

* Corresponding author. Tel./fax: +886 3 5131512.
E-mail address: changfc@mail.nctu.edu.tw (F.-C. Chang).

0032-3861/$ – see front matter © 2008 Elsevier Ltd. All rights reserved.
doi:10.1016/j.polymer.2008.06.055

treated as spheres that pack hexagonally into ordered ABCA four-layer crystals [13–17]. For norbornyl cyclopentylPOSS, the lattice constants *a* and *c* of the hexagonal array are 1.61 and 1.71 nm, respectively [17]; i.e., the lattice constant *a* is slightly larger than the diameter of norbornyl cyclopentylPOSS (ca. 1.28 nm), indicating that the side chains do not interdigitate in the solid state. When POSS molecules are covalently bonded to polymeric backbones, crystalline POSS microdomains exhibiting similar crystal reflections have been observed through XRD analysis [13,18–21].

The hydrosilylation of unsaturated monomers using octakis(dimethylsiloxy)silsesquioxane $Q_8M_8^H$ and Karstedt's catalyst (a platinum divinylsiloxane complex) has been used to yield various POSS derivatives possessing distinct functionality, including hydroxyl [22,23], polyethyleneglycol [24], liquid crystal mesogen [25], acrylate [26], and phenol [27] units. Although much literature is available highlighting the excellent performance of hydrosilylated POSS-based polymer nanocomposites, few reports have focused on why hydrosilylated POSS products are liquids or amorphous glasses, rather than crystalline materials, at room temperature. In previous studies of POSS-based nanocomposites [27,28], we observed that amorphous octakis-functionalized POSS derivatives exhibit polymer-like behavior, such as glass transition temperatures and film-formation properties. Therefore, we felt the need to investigate the properties of amorphous and crystalline POSS derivatives prior to performing further studies on POSS-based nanocomposites. In this present study, we synthesized and characterized three amorphous POSS derivatives: octakis[dimethyl(phenethyl)siloxy]silsesquioxane (OS-POSS), octakis[dimethyl(4-acetoxyphenethyl)siloxy]silsesquioxane (OA-POSS), and octakis[dimethyl(4-hydroxyphenethyl)siloxy]silsesquioxane (OP-POSS) (Fig. 1). We investigated the structures, thermal motion, and packing of these POSS derivatives using FTIR and ^{1}H NMR spectroscopy, MALDI-TOF mass spectrometry, DSC, and XRD analyses. We blended OS-POSS, OA-POSS, and OP-POSS with polystyrene (PS), poly(4-acetoxystyrene) (PAS), and poly(4-vinylpyridine) (P4VP), respectively, through solution blending in tetrahydrofuran or methanol to investigate the effects of intermolecular interactions [hydrophobic interactions between aromatic rings (OS-POSS/PS), dipole–dipole interactions between ester groups (OA-POSS/PAS), and hydrogen bonding between phenol and pyridine units (OP-POSS/P4VP)] on the dispersion of these POSS derivatives in the polymer matrices. We employed TEM and XRD analyses to determine the sizes and distributions of the POSS aggregates in these polymer nanocomposites, and TGA and DSC analyses to reveal the thermal decomposition temperatures, char yields, and glass transition temperatures of the amorphous POSS-based nanocomposites.

2. Experimental section

2.1. Materials

$Q_8M_8^H$ POSS was obtained from Hybrid Plastics. 4-Acetoxystyrene (96%), hydrazine monohydrate (98%), and platinum(0)-1,3-divinyl-1,1,3,3-tetramethyldisiloxane complex solution [Pt(dvs)] in xylene (Pt ~ 2%) were obtained from Aldrich Chemical. HPLC solvents (toluene, ethyl acetate) were used as received from TEDIA Chemical. PS, PAS, and P4VP were prepared through nitroxide-mediated radical polymerization from the unimolecular initiator (see Supplementary data for details).

2.2. Measurements

A Varian Unity Inova 500 FT NMR spectrometer was employed to obtain ^{1}H NMR spectra of samples dissolved in $CDCl_3$ or CD_3OD. A Nicolet Avatar 320 FTIR spectrometer (32 scans; resolution: 1 cm^{-1}; nitrogen purge) was used to record FTIR spectra of samples on a KBr disk. A Biflex III (Bruker Daltonics) time-of-flight mass spectrometer equipped with a 337-nm nitrogen laser was used to record MALDI-TOF mass spectra of the samples. A DuPont DSC-9000 calorimeter (scan rate: 20 °C/min; range: from −100 to +180 °C) was used to record DSC thermograms of the samples (ca. 5–10 mg) sealed in aluminum pans. The temperature and energy were indium-calibrated. The glass transition temperature was recorded as the midpoint of the specific heat increment. An M18XHF-SPA XRD spectrometer was used to collect wide-angle X-ray diffraction spectra (XRD) of samples using Co Kα radiation. The *d*-spacing distance (*d*) was transformed using Bragg's law ($\lambda = 2d \sin\theta$), where λ is the wavelength of X-rays (0.154 nm). A Hitachi H-7500 transmission electron microscope (100 kV) was used to record TEM images of the POSS-based polymer nanocomposites. The samples were ultramicrotomed at room temperature using a diamond knife on a Leica Ultracut UCT microtome apparatus to provide 70-nm-thick sections that were mounted on carbon-coated Cu TEM grids. A TA Instruments thermogravimetric analyzer (scan rate: 20 °C/min; from 30 to 800 °C; nitrogen purge: 40 mL/min) was used to record TGA thermograms of the samples positioned on a platinum holder.

2.3. Syntheses of OS-POSS and OA-POSS

Scheme 1 depicts the hydrosilylation approach used to prepare OS-POSS and OA-POSS [27,28]. A solution of $Q_8M_8^H$ (3.00 g, 2.95 mmol) and styrene (2.46 g, 23.57 mmol) or 4-acetoxylstyrene (3.98 g, 23.57 mmol) in toluene (30 mL) in a 100-mL Schlenk flask equipped with a reflux condenser and a magnetic stirrer was heated at 60 °C under argon and then Pt(dvs) (0.2 mL, 0.4 μmol) was added via syringe. The reaction, which was monitored by measuring the decrease in intensity of the FTIR spectral signal at 2134 cm^{-1} for the Si–H bonds, was complete after 4 h. The yellowish, transparent reaction mixture became clear after removal of the Pt(dvs) catalyst through flash chromatography (neutral Al_2O_3; toluene). The solvent was evaporated under reduced pressure and then the residual styrene or 4-aceoxystyrene was vacuum distilled (80 °C, 0.2 torr), to yield OS-POSS (3.45 g, 63%) or OA-POSS (3.93 g, 56%). OS-POSS is a fluid liquid at 25 °C; OA-POSS is a viscous liquid at 25 °C. Both are soluble in common organic solvents, such as tetrahydrofuran, chloroform, and acetone.

2.4. Synthesis of OP-POSS

Scheme 2 depicts the acetoxyl hydrazinolysis of OA-POSS with hydrazine monohydrate used to prepare OP-POSS [30]. OA-POSS (5.00 g, 2.16 mmol) was dissolved in 1,4-dioxane and then hydrazine monohydrate (1.73 g, 34.6 mmol, 16.0 equiv.) was added. The acetoxyl hydrazinolysis, which was monitored by measuring the decrease in intensity of the FTIR spectral signal for the C=O bond at 1762 cm^{-1}, was complete after 2 h. The solution was added dropwise into excess deionized water. The viscous OP-POSS was collected in a beaker, dissolved in ethyl acetate, dried (anhydrous $MgSO_4$), and filtered. The solvents were evaporated under vacuum at 80 °C for 4 h to yield OP-POSS (3.72 g, 87%), which is highly viscous (as a result of hydrogen bonding between the phenol units) and soluble in polar organic solvents (such as methanol).

3. Results and discussion

3.1. Syntheses of amorphous POSS derivatives

At 1:8 molar ratios of $Q_8M_8^H$ to the vinyl monomers, the hydrosilylations (Scheme 1) yielding OS-POSS or OA-POSS were complete after 4 h, as adjudged by monitoring the disappearance of

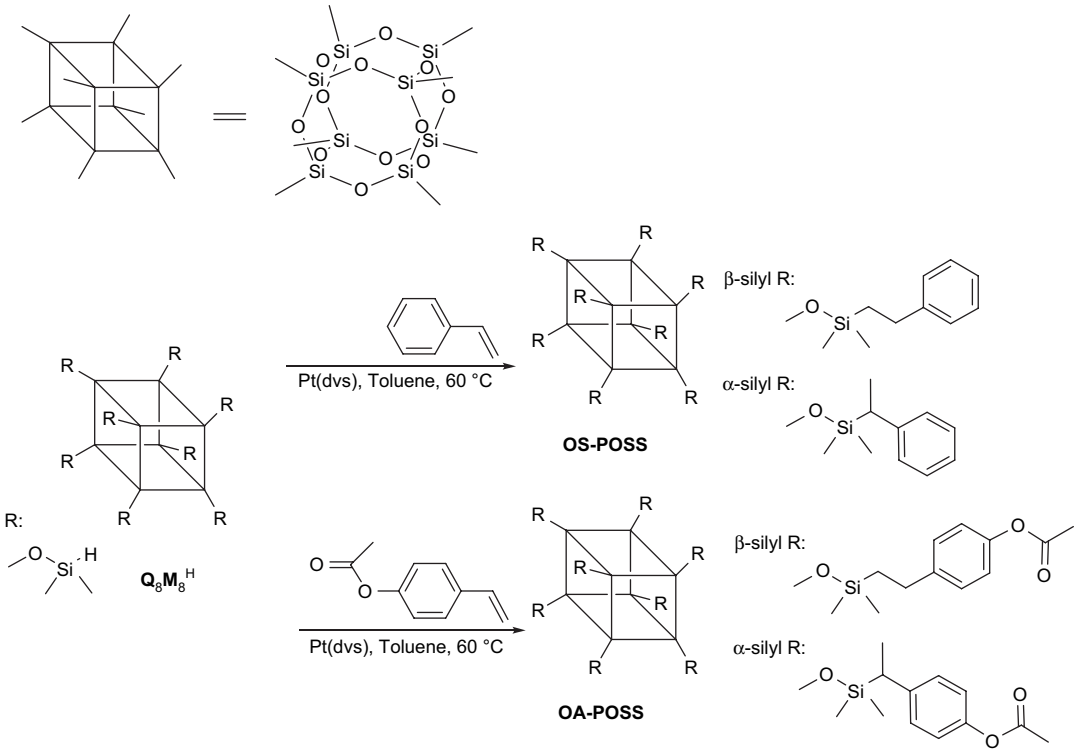

Scheme 1. Hydrosilylation of styrenic monomers with $Q_8M_8^H$ to give OS-POSS and OA-POSS.

the signals of the Si–H groups (FTIR: 2134 cm^{-1}; ^1H NMR: 4.7 ppm) in the reaction mixtures. ^1H NMR spectra of the crude products revealed the presence of only a small amount of vinyl groups (<1 mol%). OS-POSS and OA-POSS were purified through evaporation of the residual volatile styrene and 4-acetoxystyrene, respectively, under vacuum. In a previous report, we prepared OP-POSS through alkaline hydrolysis of OA-POSS with sodium hydroxide at 25 °C for 2 days [27]. Unfortunately, rearrangement of the POSS siloxane cage [27,29] and gelation reactions of the phenol groups [30] occurs when OA-POSS is hydrolyzed by sodium hydroxide over long periods of time. To overcome these problems, we noted that acetoxyl hydrazinolysis (Scheme 2) using hydrazine monohydrate could be used to selectively deprotect the acetyl groups from poly(ε-caprolactone)-*b*-poly(4-acetoxystyrene) diblock copolymers without cleaving the ester bonds of the poly(ε-caprolactone) blocks [31]. Gratifyingly, applying acetoxyl hydrazinolysis to OA-POSS at 25 °C for 2 h provided OP-POSS in high yield.

Fig. 2 displays FTIR spectra of (a) $Q_8M_8^H$, (b) OS-POSS, (c) OA-POSS, and (d) OP-POSS, obtained through solution casting onto KBr disks. The main stretching modes of these POSS derivatives appear as signals at 2134 cm^{-1} (Si–H) for $Q_8M_8^H$; at 1762 cm^{-1} (C═O) for OA-POSS; and at 3540 and 3340 cm^{-1} (free and hydrogen-bonded OH groups, respectively) for OP-POSS. A signal at 1090 cm^{-1} for Si–O–Si stretching of the POSS core is present in each spectrum, suggesting that the complete cubic structure of the siloxane cage remained unchanged during the synthesis. Fig. 3 displays MALDI-TOF mass spectra of OS-POSS, OA-POSS, and OP-POSS, obtained using 2,5-dihydroxybenzoic acid as the matrix. We observe monodisperse mass distributions of the sodiated molecular ions at 1873 g/mol for $[OS\text{-}POSS + Na]^+$, 2337 g/mol for $[OA\text{-}POSS + Na]^+$, and 2001 g/mol for $[OP\text{-}POSS + Na]^+$; the good agreement between the experimental and calculated molecular masses confirms the well-defined structures of OS-POSS, OA-POSS, and OP-POSS. Fig. 4 displays ^1H NMR spectra of $Q_8M_8^H$, OS-POSS, OA-POSS, and OP-POSS. The hydrosilylations resulted in β [$RSiCH_2CH_2R'$] and α [$RSiCH(CH_3)R'$] linkages, where R is the POSS core and R′ is the organic functional group. The molar ratios of β to α linkages were 2.22:1 and 1.82:1 for OS-POSS and OA-POSS, respectively, according to integration of the signals for the protons on the benzylic carbon atoms marked *b* (2H, β-side groups) and *b*′ (1H, α-side groups) in Fig. 1. Thus, MALDI-TOF mass spectrometry and FTIR and ^1H NMR spectrometry confirmed that the POSS products were pure, but comprised several structural isomers.

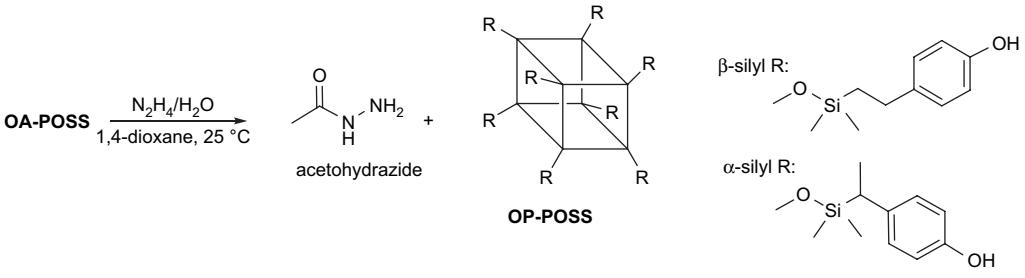

Scheme 2. Acetoxyl hydrazinolysis of OA-POSS to give OP-POSS.

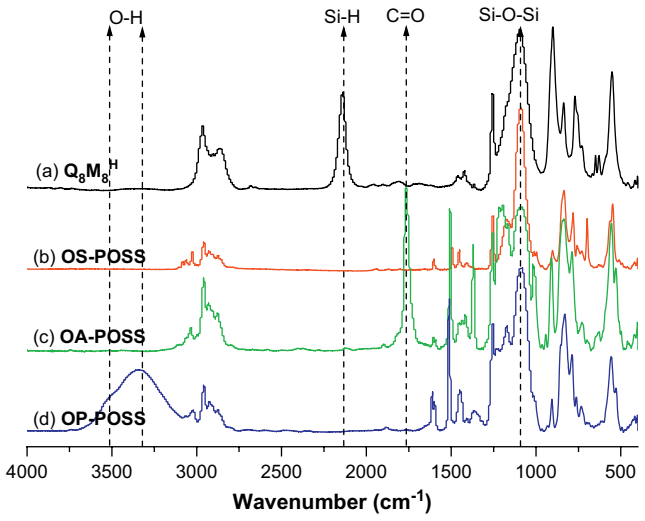

Fig. 2. FTIR spectra of (a) $Q_8M_8^H$, (b) OS-POSS, (c) OA-POSS, and (d) OP-POSS.

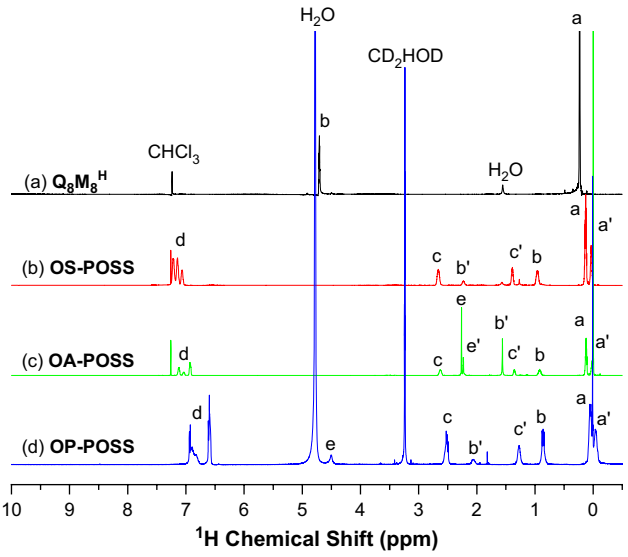

Fig. 4. ^{1}H NMR spectra of (a) $Q_8M_8^H$, (b) OS-POSS, and (c) OA-POSS in $CDCl_3$ and of (d) OP-POSS in CD_3OD.

3.2. Characterization of amorphous POSS derivatives

Fig. 5 displays DSC thermograms of $Q_8M_8^H$ during the first heating process and of OS-POSS, OA-POSS, and OP-POSS during the second heating process. The transition of $Q_8M_8^H$ from crystalline to glass occurred at 104.3 °C. With its absence of interdigitated side groups in the crystal (lattice constant $a >$ molecular size) [17,36], we attribute this low transition temperature of $Q_8M_8^H$ to intramolecular rotation resulting in the isotropic glass (see Fig. S5 in Supplementary data, for a polarized optical microscopy image). After hydrosilylation, the amorphous POSS derivatives OS-POSS, OA-POSS, and OP-POSS revealed glass transition temperatures (T_g) of −51.8, −14.2, and +18.7 °C, respectively, in their DSC thermograms. We attribute the increments in T_g to the increased strength of the intermolecular interaction upon proceeding from OS-POSS (van der Waals forces) to OA-POSS (dipole–dipole interactions) to OP-POSS (phenol–phenol hydrogen bonding). For amorphous polymers, the glass transition typically occurs from a disordered glassy state to a viscous liquid as a result of disorderly thermal motions of polymer segments during thermal treatment. In this similar case, the coexistence of several isomers of these hydrosilylated POSS derivatives is responsible for the disordered aggregation (glassy state) and has similar glass transition observed by DSC thermograms.

Fig. 6 displays XRD patterns of $Q_8M_8^H$, OA-POSS, and OP-POSS at 25 °C (note that OS-POSS was not a suitable subject for XRD analysis because of its high fluidity). The major diffraction peaks (and planes) expected for ABCA rhombohedral crystal structures appear for the crystalline $Q_8M_8^H$ at 8.13° (101), 10.67° (110), 11.86° (102), and 18.54° (113), similar to those of most POSS crystals [12–17]. After hydrosilylation, the POSS products, which are liquids at 25 °C, display three amorphous halos for three d-spacing distances (d_1, d_2, and d_3; Fig. 7a). Both d_1 and d_2 have been observed previously for amorphous poly(silsesquioxane); they are assigned to the width of each ladder-like double chain (Si–O–Si; d_1 in Fig. 7b) and the distance between two adjacent ladder-like double chains (Si–R/R–Si; d_2 in Fig. 7b) [33,35]. Because POSS can be regarded as a cyclic tetramer of poly(silsesquioxane), as indicated in Fig. 7, we assign the two distinct amorphous halos of OA-POSS and OP-POSS at 24.10° (d-spacing of ca. 0.37 nm) and 17.51° (d-spacing of ca. 0.51 nm) to the Si–O–Si distance (d_1 = ca. 0.33 nm) and the diameter of the POSS siloxane cage (d_3 = ca. 0.53 nm; Figs. 7a and 8a),

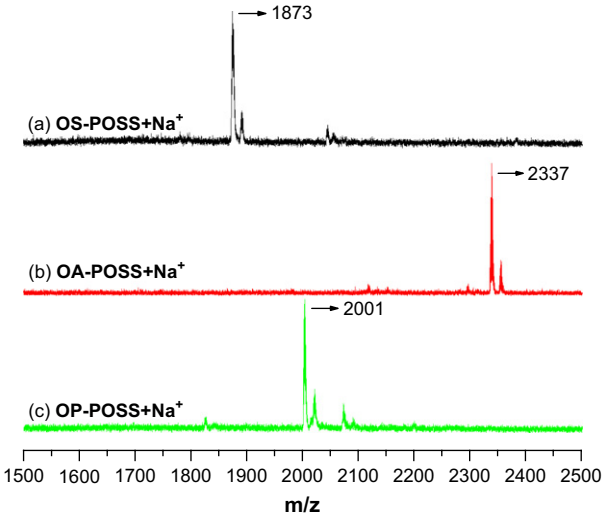

Fig. 3. MALDI-TOF mass spectra of (a) OS-POSS, (b) OA-POSS, and (c) OP-POSS.

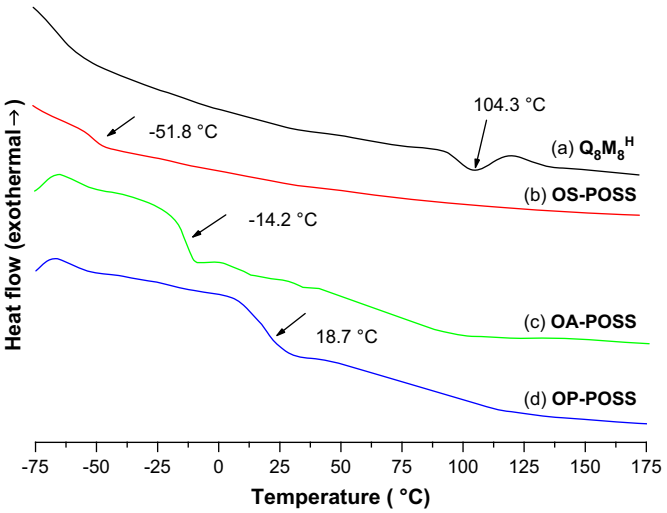

Fig. 5. DSC thermograms of (a) $Q_8M_8^H$, (b) OS-POSS, (c) OA-POSS, and (d) OP-POSS.

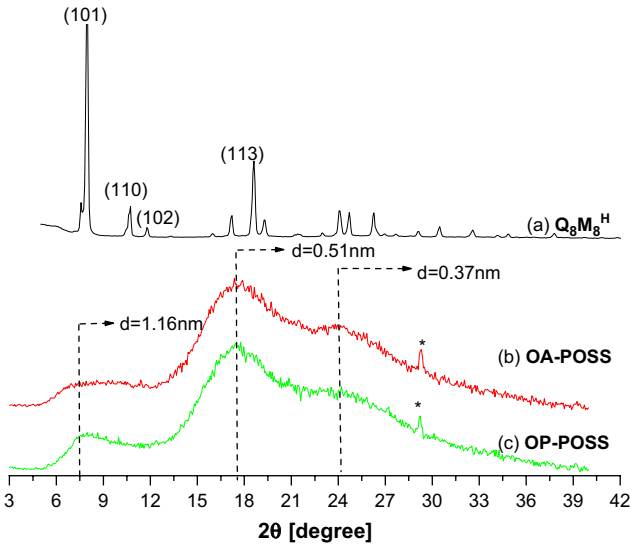

Fig. 6. XRD patterns of (a) $Q_8M_8^H$, (b) OA-POSS, and (c) OP-POSS. Asterisks mark the signals from the holder.

respectively [32–34]. The peak at 17.51° once again confirms the intact cage structures of the amorphous POSS derivatives. We used CS Chem3D software (MM2 calculations) for molecular modeling to calculate the cube size (ca. 0.53 nm, Fig. 8a) and the lengths of the hydrosilylated ethylene groups (β and α forms). The end-to-end lengths (Fig. 8b–e) are 1.30 nm for the β-side chain of OA-POSS, 0.97 nm for the α-side chain of OA-POSS, 1.09 nm for the β-side chain of OP-POSS, and 0.76 nm for the α-side chains of OP-POSS. For OA-POSS, the value of 7.62° in Fig. 6b corresponds to a distance between two adjacent POSS cores (d_3) of ca. 1.16 nm. This distance approaches the average of the end-to-end lengths of the β- and α-side chains on OA-POSS (*d*-spacings of ca. 1.30 and 0.97 nm, respectively; Fig. 8b and c). This distance of 1.16 nm indicates that attractive interactions between POSS cores promotes POSS aggregation with interdigitation of the coexisting linear (β) and branched (α) side chains on OA-POSS, in stark contrast to the lack of interdigitation of the side groups of POSS crystals. Although the calculated length of the β side chains on OP-POSS is 1.09 nm (Fig. 8d), the OP-POSS peak at 7.62° is relatively sharp in Fig. 6c, reflecting the more uniform and non-interpenetrating intermolecular *d*-space caused by phenol–phenol hydrogen bonding. We attribute the high glass transition temperature of OP-POSS mostly to the formation of strong intermolecular hydrogen bonds, even though their intermolecular distances are also increased. The hydrogen bonding of OP-POSS can be further evidenced in temperature-dependent FTIR spectra (see Fig. S6 in Supplementary data).

3.3. POSS-based polymer nanocomposites

We prepared three POSS-based nanocomposites incorporating 20 wt% POSS through solution blending of OS-POSS and polystyrene (OS-POSS/PS) in THF, OA-POSS and poly(4-acetoxystyrene) (OA-POSS/PAS) in THF, and OP-POSS and poly(4-vinylpyridine) (OP-POSS/P4VP) in MeOH (see Figs. S1–S4 of Supplementary data for the synthesis and characterization of these polymers). THF and MeOH served as good solvents for premixing the POSS derivatives and polymers because of their strong solvent–POSS and solvent–polymer interactions. Thermodynamically, the dispersion or aggregation of POSS molecules is determined by the mixture entropy and mixture enthalpy: the former represents the extent of POSS dispersion (high molar mass polymers can be neglected) and the latter represents the balance of the strengths of the POSS–POSS, POSS–polymer, and polymer–polymer interactions. To elucidate the microstructures of OS-POSS/PS, OA-POSS/PAS, and OP-POSS/P4VP, we directly observed images of their microtomed POSS composites. Fig. 9 displays TEM images and schematic microstructures of the POSS-based polymer nanocomposites. Image contrast in a TEM micrograph originates from the different degrees of electron scattering from light and heavy atoms. The aggregated POSS siloxane cages appear as dark spots in the gray polymer medium comprised solely of carbon and hydrogen atoms. Wu et al. [32] reported TEM images displaying individual POSS molecules (sizes: 1.5–3.0 nm) covalently bonded onto PS chains. In contrast, our octakis-functionalized amorphous POSS derivatives are dispersed through physical intermolecular interactions between their outer organic units and the organic polymer matrices. Thus, the size and distribution of the POSS aggregates depend strongly on the type and strength of the intermolecular interactions. As is evident in Fig. 9a–c, OS-POSS aggregates having rough sizes of 100-nm-diameters were well dispersed in the PS matrix. Clearly, the weak aromatic hydrophobic interactions between OS-POSS and PS cannot overcome the attraction of the POSS cores, even though premixing (solution blending) promoted uniform dispersion of the POSS derivatives. With their stronger intermolecular dipole–dipole interactions, the dark OA-POSS aggregates are absent (i.e., the units are well dispersed) in the PAS matrix (Fig. 9d–f). The improved homogeneity of the OA-POSS/PAS system is driven thermodynamically by the mixture entropy, namely through the similar strengths of the OA-POSS–PAS and POSS–POSS intermolecular interactions. For the mixture of OP-POSS and P4VP, which features strong phenol–pyridine hydrogen bonds, we observed both dispersed and aggregated OP-POSS units in the matrix, resulting presumably from competition between hydrogen bonds of similar strength (phenol–pyridine and phenol–phenol). The polar P4VP can be dissolved in methanol based on the hydrogen bond between hydroxyl and pyridine. We supposed that the hydrogen bonds between high concentration OP-POSS and P4VP result in the relatively low solubility [37]. Thus, OP-POSS aggregation was observed by TEM images (Fig. 9g–i). After N_2-purged thermal annealing at 180 °C for 1 h, OP-POSS aggregation in the P4VP medium becomes smaller than that before treatment (see Supplementary data). Consequently, it appears that the dipole–dipole interaction is the optimal noncovalent interaction with which polymer nanocomposites can be obtained incorporating well-dispersed amorphous POSS units. Fig. 10 presents XRD patterns of OA-POSS, PAS, OA-POSS/PAS, OS-POSS/PS, and OP-POSS/P4VP. The signal for

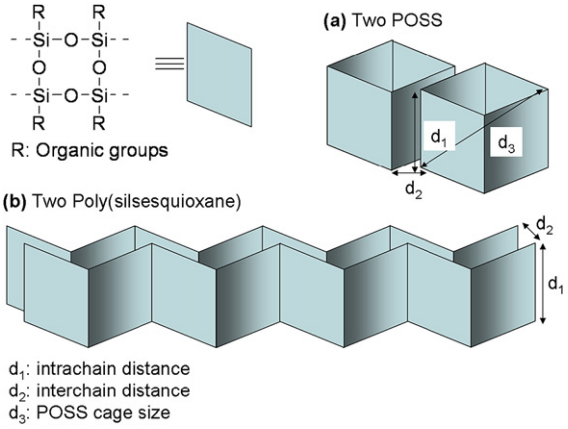

Fig. 7. Geometric drawings of (a) two POSS cages and (b) two poly(silsesquioxane) chains. Arrows mark the intra-chain distance (d_1), the inter-chain distance (d_2), and the size of a POSS cage (d_3).

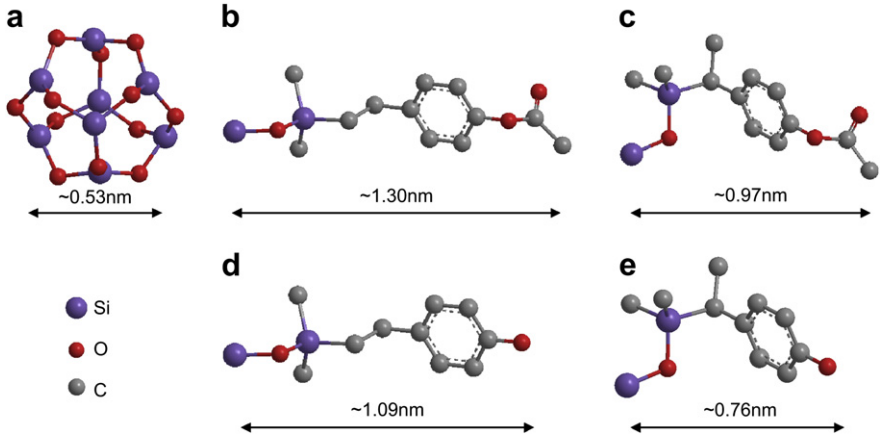

Fig. 8. Chem3D MM2 calculations and 3D structures of (a) a POSS core, (b) the β side chain of OA-POSS, (c) the α side chain of OA-POSS, (d) the β side chain of OP-POSS, and (e) the α side chain of OP-POSS.

OA-POSS aggregation at 7.62° is absent for OA-POSS/PAS, confirming the high dispersion of OA-POSS in the PAS matrix. For OS-POSS/PS and OP-POSS/P4VP, however, the signal for POSS aggregations is present at 7.62° (Fig. 10d and e).

Table 1 summarizes the molar masses and thermal properties of the POSS derivatives, the polymers, and their composites. Fig. 11 displays TGA thermograms of OS-POSS, PS, OS-POSS/PS, OA-POSS, PAS, OA-POSS/PAS, OP-POSS, P4VP, and OP-POSS/P4VP. For P4VP and OP-POSS/P4VP, residual polar methanol was removed by keeping in vacuum oven at 100 °C for 1 h. Among the three amorphous POSS derivatives (Fig. 11a, d and g; Table 1), OS-POSS possesses the highest thermal stability with its onset point at 431.7 °C; its char yield of only 10.3 wt% is less than its 42 wt% siloxane content. Thus, it appears that decomposition of the organic components of OS-POSS can promote further siloxane degradation, resulting in the low char yield. In contrast, OA-POSS and OP-POSS

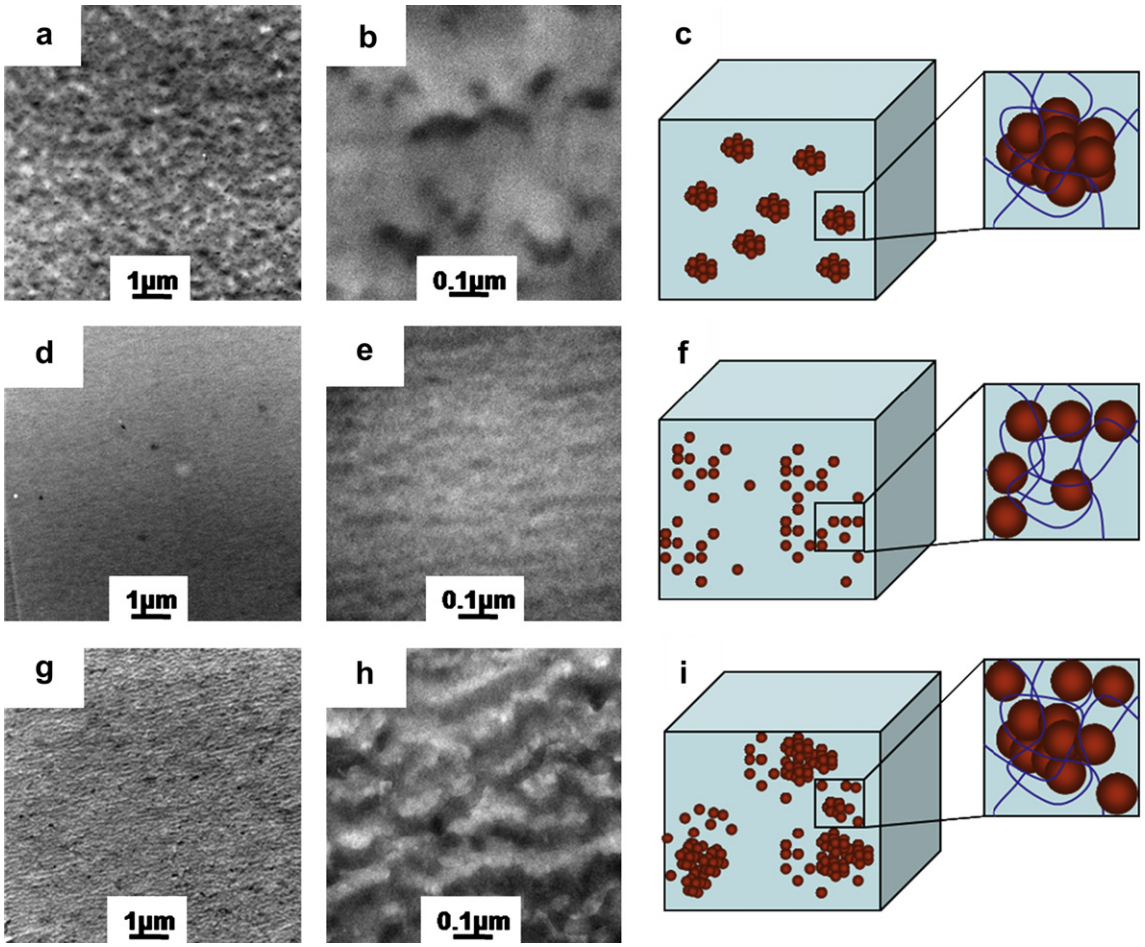

Fig. 9. TEM images and schematic microstructures of POSS-based polymer nanocomposites (a–c) OS-POSS/PS, (d–f) OA-POSS/PAS, and (g–i) OP-POSS/P4VP. Three samples were treated by N_2-purged thermal annealing at 180 °C for 1 h.

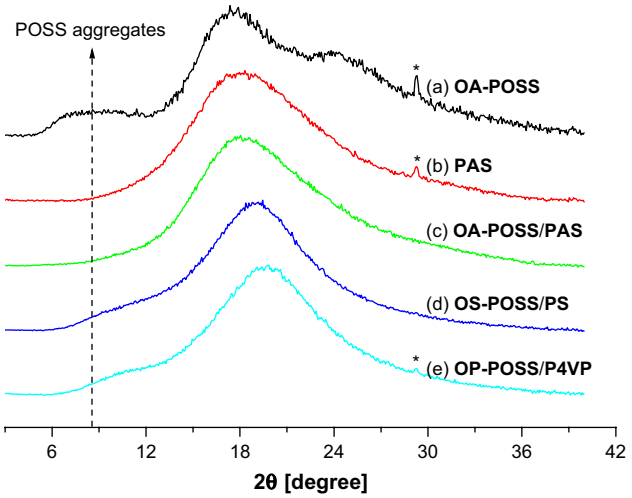

Fig. 10. XRD patterns of (a) OA-POSS, (b) PAS, (c) OA-POSS/PAS, (d) OS-POSS/PS, and (e) OP-POSS/P4VP. Asterisks mark the signals of the holder.

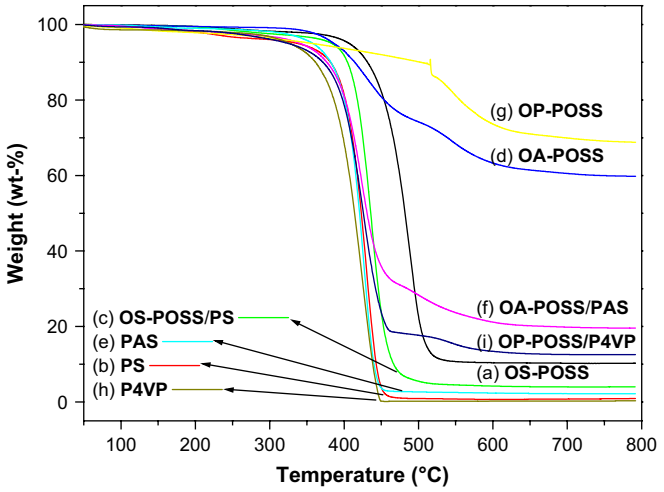

Fig. 11. TGA thermograms of (a) OS-POSS, (b) PS, (c) OS-POSS/PS, (d) OA-POSS, (e) PAS, (f) OA-POSS/PAS, (g) OP-POSS, (h) P4VP, and (i) OP-POSS/P4VP. The residual methanol in samples of P4VP and OP-POSS/P4VP was removed by vacuum distillation at 100 °C for 1 h.

have higher char yields (60.6 and 70.1 wt%, respectively) because their phenol units tend to form aromatic char structures, rather than small molecular vapors, at temperatures above their decomposition temperatures (384.1 and 358.5 °C, respectively). Depolymerization of the common polymers PS, PAS, and P4VP (Fig. 11b, e and h; Table 1) occurs from the chain ends at their decomposition temperatures, resulting in low char yields. After incorporating the POSS derivatives into these polymers (Fig. 11c, f and i; Table 1), the char yields of OS-POSS/PS and OP-POSS/P4VP (4.1 and 12.6 wt%, respectively) were slightly higher than the theoretical values (2.7 and 12.4 wt%, respectively) calculated for a weight average of 20 wt% POSS derivative and 80 wt% polymer, but, interestingly, in comparison with the theoretical char yield by weight-average method as listed in Table 1, the char yield of OA-POSS/PAS increased by ca. 5.9 wt% (=19.8–13.9) which is more than three times the char yield increase of OS-POSS/PS (1.4 wt%) or OP-POSS/P4VP (0.2 wt%). This result can be interpreted as the well-dispersed OA-POSS forming a larger contact interface with PAS, thereby incorporating more PAS segments in the aromatic char structure. Fig. 12 displays DSC thermograms of PS, OS-POSS/PS, PAS, OA-POSS/PAS, P4VP, and OP-POSS/P4VP. Because a glass transition reflects local thermal motion within several repeat units, a new glass transition temperature after incorporation of 20 wt% POSS into a polymer matrix suggests the formation of a composite microstructure. Thus, competition among multiple intermolecular interactions for POSS, the polymer, and the solvent directly affects the dispersion and aggregation of the composites after evaporation of the solvent, as was revealed in the TEM images. Therefore, the disappearance of glass transitions for the pure POSS derivatives indicates that the dark aggregation domains (Fig. 9) were composed of POSS and polymer composites. The presence of the POSS derivatives expanded the interspaces (increased the free volume) between the polymer chains, resulting in lower glass transition temperatures. Thus, we observed a single glass transition of OS-POSS/PS nanocomposite at 72.1 °C. For the OP-POSS/P4VP nanocomposite, the strong phenol–pyridine hydrogen bonds compensate for the high mobility in the interspaces between the OP-POSS units and the P4VP chains, resulting in a high glass transition temperature (121.9 °C) approaching that of the pristine P4VP (129.0 °C). Interestingly, the medium-strength dipole–dipole interactions in the OA-POSS/PAS nanocomposite resulted in a decrease of the glass transition temperature by 36 °C, a considerably larger drop than those for

Table 1
Molar masses and thermal properties of POSS derivatives, polymers, and their composites

Entry	Molar mass		Decomposition[d]		Glass transition[h]	
	M_n (g/mol)	M_w (g/mol)	Onset (°C)	Char[e] (wt%)	Initial (°C)	Median (°C)
OS-POSS	1850[b]	1850[b]	431.7	10.3	−55.5	−51.8
OA-POSS	2314[b]	2314[b]	384.1	60.6	−18.2	−14.2
OP-POSS	1978[b]	1978[b]	358.5[f]	70.1	10.2	18.7
PS	7522[c]	9932[c]	388.9	0.8	85.3	90.8
PAS	24 532[c]	38 436[c]	395.4	2.2	116.4	124.8
P4VP	4693[c]	7002[c]	377.2	0.3	117.9	129.0
OS-POSS/PS[a]	–	–	414.6	4.1 (2.7[g])	66.8	72.1
OA-POSS/PAS[a]	–	–	386.2	19.8 (13.9[g])	80.3	93.5
OP-POSS/P4VP[a]	–	–	392.5	12.6 (12.4[g])	112.9	121.9

[a] Containing 20 wt% POSS derivatives.
[b] Obtained from MALDI-TOF mass spectra.
[c] Obtained from RI-GPC with DMF elution (0.6 mL/min) and PS calibration (see Supplementary data).
[d] Obtained from TGA thermograms (heating rate: 20 °C/min).
[e] Recorded at 700 °C.
[f] Recorded at 5 wt% loss.
[g] Calculated from a weight average of 20 wt% POSS derivative and 80 wt% polymer.
[h] Obtained from the second run of the DSC thermogram (heating rate: 20 °C/min).

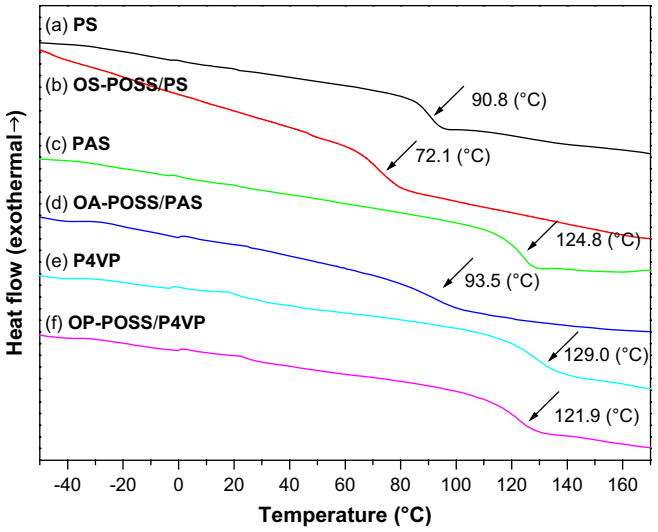

Fig. 12. DSC thermograms of (a) PS, (b) OS-POSS/PS, (c) PAS, (d) OA-POSS/PAS, (e) P4VP, and (f) OP-POSS/P4VP.

the OS-POSS/PS and OP-POSS/P4VP nanocomposites. The well-dispersed OA-POSS units result in much greater contact in the interspaces of PAS, thereby expanding the free volume between polymer segments.

4. Conclusion

The polymer-like glass transition of amorphous POSS derivatives, such as OS-POSS, OA-POSS, or OP-POSS, has rarely been mentioned in the literature; indeed, they are usually regarded as pure liquids possessing melting points below 25 °C. Thus, aggregation of such amorphous POSS derivatives in polymer matrices is not expected to result in crystal-like lamellar microstructures. In this study, we improved upon our previous methods for preparing monodisperse OS-POSS, OA-POSS, and OP-POSS, but β ($RSiCH_2CH_2R'$) and α [$RSiCH(CH_3)R'$] linkages (R is the POSS core and R′ is an organic functional group) resulted in multiple conformational isomers of amorphous POSS products. The distinct geometries of these isomers inhibit the POSS derivatives' crystallization; thus, these nanosized POSS molecules without restriction in the crystal lattice exhibit high conformational flexibility. As a result, intermolecular interactions have a great effect on their polymer-like glass transition temperatures. When incorporated into polymer blends, the distribution of the POSS derivatives and their effects on the blends' properties are also dependent upon the specific intermolecular interactions that are present. Among three types of noncovalent interaction – aromatic hydrophobic interactions of OS-POSS/PS, dipole–dipole interactions of OA-POSS/PAS, and phenol–pyridine hydrogen bonds of OP-POSS/P4VP – the dipole–dipole interaction between the acetyl groups is the best selection to disperse 20 wt% amorphous POSS in the polymer matrices. As a consequence, amorphous POSS cages can be well dispersed in the polymeric medium through the intermolecular interaction, which have similar strength to the POSS–POSS attractive interaction.

Acknowledgment

We thank Dr. Y.-C. Chen and Dr. C.-S. Lee of the Institute of Applied Chemistry, National Chiao Tung University, for assistance in recording the MALDI-TOF mass spectra and the XRD patterns. This study was supported financially by the National Science Council, Taiwan, Republic of China, under contract no. NSC-95-2216-E-009-018 and by the Ministry of Education's "Aim for the Top University" program.

Appendix. Supplementary data

Supplementary data associated with this article can be found in the online version, at doi:10.1016/j.polymer.2008.06.055.

References

[1] Giannelis EP. Adv Mater 1996;8:29–35.
[2] Vo LT, Giannelis EP. Macromolecules 2007;40:8271–6.
[3] Bansal A, Yang H, Li C, Benicewicz BC, Kumar SM, Schadler LS. J Polym Sci Part B Polym Phys 2006;44:2944–50.
[4] Lu X, Chao D, Chen J, Zhang W, Wei Y. Mater Lett 2006;60:2851–4.
[5] Lu X, Yu Y, Chen L, Mao H, Gao H, Wang J, et al. Nanotechnology 2005;16:1660–5.
[6] Huang JC, He CB, Xiao Y, Mya KY, Dai J, Siow YP. Polymer 2003;44:4491–9.
[7] Baney RH, Itoh M, Sakakibara A, Suzuki T. Chem Rev 1995;95:1409–30.
[8] Laine RM. J Mater Chem 2005;15:3725–44.
[9] Schwab JJ, Lichtenhan JD. Appl Organometal Chem 1998;12:707–13.
[10] Voronkov MG, Lavrent'ev V. Top Curr Chem 1982;102:199–236.
[11] Feher FJ, Budzichowski TA. J Organometal Chem 1989;373:153–63.
[12] Sheng YJ, Lin WJ, Chen WC. J Chem Phys 2004;121:9693–701.
[13] Fu BX, Hsiao BS, Pagola S, Stephens P, White H, Rafailovich M, et al. Polymer 2001;42:599–611.
[14] Cui L, Collet JP, Xu G, Zhu L. Chem Mater 2006;18:3503–12.
[15] Larsson K. Ark Kemi 1960;16:203–8.
[16] Larsson K. Ark Kemi 1960;16:209–14.
[17] Waddon AJ, Coughlin EB. Chem Mater 2003;15:4555–61.
[18] Zheng L, Waddon AJ, Farris RJ, Coughlin EB. Macromolecules 2002;35:2375–9.
[19] Waddon AJ, Zheng L, Farris RJ, Coughlin EB. Nano Lett 2002;2:1149–55.
[20] Carroll JB, Waddon AJ, Nakade H, Rotello VM. Macromolecules 2003;36:6289–91.
[21] Zheng L, Hong S, Cardoen G, Burgaz E, Gido SP, Coughlin EB. Macromolecules 2004;37:8606–11.
[22] Zhang C, Laine RM. J Am Chem Soc 2000;122:6979–88.
[23] Kim KM, Inakura T, Chujo Y. Polym Bull 2001;46:351–6.
[24] Maitra P, Wunder SL. Chem Mater 2002;14:4494–7.
[25] Zhang C, Bunning TJ, Laine RM. Chem Mater 2001;13:3653–62.
[26] Sellinger A, Laine RM. Macromolecules 1996;29:2327–30.
[27] Lin HC, Kuo SW, Huang CF, Chang FC. Macromol Rapid Commun 2006;27:537–41.
[28] Kuo SW, Lin HC, Huang WJ, Huang CF, Chang FC. J Polym Sci Part B Polym Phys 2006;44:673–86.
[29] Lichtenhan JD, Haddad TS, Feher FJ, Soulivong D. U.S. Patent 6,770,724; Aug 3 2004.
[30] Chen X, Jankova K, Kops J, Batsberg W. J Polym Sci Part A Polym Chem 1999;37:627–33.
[31] Kuo SW, Huang CF, Lu CH, Jeong KU, Chang FC. Macromol Chem Phys 2006;207:2006–16.
[32] Wu J, Haddad TS, Kim G-M, Mather PT. Macromolecules 2007;40:544–54.
[33] Imae I, Kawakmi Y. J Mater Chem 2005;15:4581–3.
[34] Zhang J, Xu R, Yu D. Eur Polym J 2007;43:743–52.
[35] Liu C, Liu Y, Shen Z, Xie P, Dai D, Zhang R, et al. Macromol Chem Phys 2001;202:1576–80.
[36] Liu L, Tian M, Zhang W, Zhang L, Mark JE. Polymer 2007;48:3201–12.
[37] Kuo SW, Tung PH, Chang FC. Macromolecules 2006;39:9388–95.